Structure of Aqueous Solutions of Ions and Neutral Solutes at Infinite Dilution at a Supercritical Temperature of 683 K

Jayendran C. Rasaiah,* Jerzy P. Noworyta, and S. Koneshan

Contribution from the Department of Chemistry, University of Maine, Orono, Maine 04469

Received June 5, 2000. Revised Manuscript Received September 13, 2000

Abstract: We discuss the structure of alkali metal ions, halide ions, and uncharged solutes at infinite dilution in supercritical water solutions, at solvent densities of 0.35, 0.20, and 0.997 g cm^{-3} at a temperature of 683 K using the SPC/E model for water. This model has critical constants (T_c = 640 K, ρ_c = 0.29 g cm^{-3}) which compare well with the corresponding values (T_c = 647 K, ρ_c = 0.322 g cm^{-3}) for real water. The solute−water pair correlation functions are qualitatively different for the charged and uncharged solutes at 683 K at both 0.35 and 0.20 g cm^{-3} solvent densities, with water expelled from the immediate vicinity of the uncharged solute but retained and compressed in the neighborhood of a small ion. Increasing the solvent density to 0.997 g cm^{-3} at 683 K leads to dramatic changes in the solvent structure around an uncharged solute, with the formation of hydrogen-bonded cages analogous to those observed at room temperature (298 K) at the same solvent density. The primary hydration numbers of the ions at 683 K and solvent density of 0.35 g cm^{-3} are nearly the same as the corresponding values at room temperature at a solvent density of 0.997 g cm^{-3}. The partial molar volumes of the ions and uncharged species at the supercritical temperature are different in sign and are explained in terms of a simple model. The dynamics of ions and uncharged solutes under the same supercritical conditions are discussed in the companion to this paper.

1. Introduction

Supercritical fluids have played an important role in a wide variety of applications over the past decade due to their high dissolving power combined with enhanced mass transport.[1−4] The unique properties of supercritical fluids are generally attributed to high compressibility and fluctuations in the density, creating voids and clusters. The density is easily fine-tuned through small changes in the temperature or pressure in the supercritical region. However, a detailed microscopic explanation of the behavior of supercritical solutions and neat solvents at the molecular level, taking account of both atomic correlations and density fluctuations, is still lacking, although there have been many studies and considerable progress made recently.[5−10]

Studies of aqueous solutions under ambient conditions,[11] i.e., room temperature and a water density of 0.997 g cm^{-3}, support the view that the structure and the dynamics of ions in aqueous solutions require explicit consideration of the charge asymmetry of the water molecule. One of the main goals of this study is to see how these are affected by extreme changes in temperature and density. We investigate this by comparing the properties of the same solutes in aqueous solution under widely different conditions of temperature and solvent density, to see whether supercritical conditions enhance or reduce the differences in the equilibrium and transport properties of solutes of different size and charge observed at room temperature.

Experimental measurements of the partial molar volume and enthalpy of dissolved solutes have suggested dramatic alterations in the solvent structure around the solute when the temperature is raised above the critical point. This has led to the interpretation of the large negative partial molar volumes $\overline{V_2^\infty}$ of ionic solutes at infinite dilution in the supercritical region as due to electrostriction and clustering of the solvent around the solute. Large positive values of $\overline{V_2^\infty}$ of nonpolar solutes are attributed to the opposite effect of solvent depletion in the immediate vicinity of the solute. Both solvent clustering and depletion are also observed in computer simulations of charged and uncharged solutes in supercritical solvents.[7] Their significance is complicated and obscured by the large solvent density fluctuations that dominate the divergence of the solute partial molar volumes and enthalpies at the critical point and are important even at supercritical temperatures.

* To whom correspondence should be addressed. E-mail: rasaiah@maine.edu.

(1) (a) Kiran, E., Levelt Sengers, J. M. H., Eds. *Supercritcal Fluids Fundamentals and Applications*; NATO ASI Series 271; Kluwer Academic Publishers: Dordrecht, The Netherlands, 1994. (b) Levelt Sengers, J. M. H. Thermodynamics of Solutions Near the Solvent's Critical Temperature. In *Supercritical Fluid Technology: Reviews in Modern Theory and Applications*; Bruno, T. J., Ely, J. F., Eds.; CRC Press: Boston, 1991.

(2) Fernadez-Prini, R.; Japas, M. L. *Chem. Soc. Rev.* **1994**, *23*, 155.

(3) Eckert, C. A.; Knuston, B. L,; Debenedetti, P. G. *Nature* **1996**. *383*, 313.

(4) Tucker, S. C.; Maddox, M. W. *J. Phys. Chem. B* **1998**, *102*, 2437.

(5) (a) Anisimov, M. A.; Sengers, J. V. Crossover Critical Phenomena in Aqueous Solutions. Presented at the 13th International Conference on Properties of Water and Steam, Toronto, Canada, 1999. (b) Povodyrev, A. A.; Anisimov, M. A.; Sengers, J. V.; Marshall, W. M.; Levelt Sengers, J. M. H. *Int. J. Thermophys.*, in press. (c) Povodyrev, A. A.; Anisimov, M. A.; Sengers, J. V.; Marshall, W. M. Levelt Sengers, J. M. H. *Physica A* **1997**, *244*, 298.

(6) (a) Guissani, Y.; Guillot, B. *J. Chem. Phys*. **1993**, *98*, 8221. (b) Guillot, B.; Guissani, Y. *J. Chem. Phys*. **1993**, *99*, 8075.

(7) (a) Chialvo, A. A.; Cummings, P. T. Molecular Simulation of Supercritical Water and Aqueous Solutions, to be published (preprint). (b) Chialvo, A. A.; Cummings, P. T. *AIChE J.* **1994**, *40*, 1558.

(8) Balbuena, P. B.; Johnston, K. P.; Rossky, P. J. *J. Phys. Chem*. **1996**, *100*, 2706, *J. Phys. Chem*. **1996**, *100*, 2705.

(9) Balbuena, B.; Johnston, K. P.; Rossky, P. J.; Hyun, J. K. *J. Phys. Chem. B* **1998**, *102*, 3806.

(10) Tucker, S. *Chem. Rev.* **1999**, *91*, 399.

(11) (a) Lee, S. H.; Rasaiah, J. C. *J. Phys. Chem*. **1996**, *100*, 1420. (b) Koneshan, S.; Rasaiah, J. C.; Lynden-Bell, R. M.; Lee, S. H. *J. Phys. Chem.* **1998**, *102*, 4193 (c) Koneshan, S.; Lynden-Bell, R. M.; Rasaiah, J. C. *J. Am. Chem. Soc.* **1998**, *120*, 12041.

10.1021/ja001978z CCC: $19.00
Published on Web 10/27/2000

In this paper and the one following,[33] we begin a study of the equilibrium and transport properties of charged and neutral solutes at infinite dilution under supercritical conditions. The temperature chosen for our studies is 683 K, nearly 40 degrees above the critical temperature of water, while the solvent density is, for most of our work, 0.35 g cm^{-3}, which is close to the critical density of 0.32 g cm^{-3} . Here we discuss in detail the solute−water distribution functions and the hydration numbers, as well as the partial molar volumes of charged and neutral solutes. Additional results for a few ions and uncharged solutes at 0.20 and 0.997 g cm^{-3} are presented at 683 K in order to study the effect of solvent density on the structure. In the following paper[33] we discuss the residence times of water in the first hydration shell, solvation dynamics of ions, and the diffusion of ions and uncharged species at infinite dilution at 683 K. In another paper, we report on our simulation studies of the diffusion and association of ions in sodium chloride solutions at finite concentrations.[12] A review of our studies of the structure and dynamics of ions and nonpolar solutes in water at ambient and supercritical temperatures will appear elsewhere.[13]

2. Model

The systems of interest in our work are infinitely dilute aqueous solutions under supercritical conditions. Interionic interactions, characteristic of ionic solutions at finite concentrations, are absent at infinite dilution. The behavior of these solutions is determined by the interactions between solute and solvent as well as between the solvent molecules. In practice, a single solute particle and 511 water molecules are treated explicitly in a cubic simulation cell, with periodic boundary conditions and minimum image convention applied in the standard way. In addition, we performed simulations of pure water under the same conditions and compared its properties (namely, potential energy, and distribution functions) with those in the bulk when the solute was present, to clarify and quantify the behavior of the solvent in solutions at infinite dilution. These last results are also used in calculating water−water correlation functions in our determination of the partial molar volumes of the solutes. We also studied a smaller system of 215 molecules of water and one solute in a few simulations to investigate the effect of sample size and the correlation length on the measured equilibrium properties. This is discussed in the next section.

We used the extended simple point charge (SPC/E) model for water[14] and the ion−water parameters developed by Dang et al.[15] (see Table 1) and employed by us[11,16] in previous studies of ion and neutral solute diffusion coefficients at room temperature. The SPC/E model for water, whose description follows, is a reparametrization of a simple point charge (SPC) representation that corrects for the self-polarization energy of induced dipoles at 298 K by adjusting the charges.

The water molecule in the SPC/E model is treated as a collection of simple point charges distributed over the atomic sites with Lennard-Jones interactions between the oxygen atoms.

Table 1. Halide−Water, Alkali Metal Cation−Water, and Water−Water Potential Parameters (SPC/E Model)[a]

species	σ_{io} (Å)	ϵ_{io} (kJ/mol)	charge q
F^-	3.143	0.6998	−1
Cl^-	3.785	0.5216	−1
I^-	4.168	0.5216	−1
Li^{+b}	2.337	0.6700	+1
Na^+	2.876	0.5216	+1
Rb^+	3.348	0.5216	+1
Cs^+	3.526	0.5216	+1
water	σ_{oo} (Å)	ϵ_{oo} (kJ/mol)	charge q
$O(H_2O)$	3.169	0.6502	−0.8476
$H(H_2O)$			+0.4238

[a] In the SPC/E model for water, the charges on H are at 1.000 Å from the Lennard-Jones center at O. The negative charge is at the O site and the HOH angle is 109.47°. [b] The Li^+ parameters are for the revised polarizability (RPOL) model.

The OH bond distances are constrained at 1.0 Å. The bond angle between the two OH bonds is fixed at 109.47°. The intermolecular interaction between a pair of water molecules is given by

$$u_{water} = 4\epsilon_{oo}\left[\left(\frac{\sigma_{oo}}{r_{oo}}\right)^{12} - \left(\frac{\sigma_{oo}}{r_{oo}}\right)^{6}\right] + \frac{1}{4\pi\epsilon_0}\sum_{i=1}^{3}\sum_{j=1}^{3}\frac{q_i q_i}{r_{ij}} \qquad (2.1)$$

The first term is a Lennard-Jones potential between the oxygen sites of individual water molecules, and the second term is the electrostatic term in which q_i is the charge on site i and r_{ij} is the distance between sites i and j on two different water molecules. The ion−water potential used in our studies has a similar form:

$$u_{io} = 4\epsilon_{io}\left[\left(\frac{\sigma_{io}}{r_{io}}\right)^{12} - \left(\frac{\sigma_{oo}}{r_{oo}}\right)^{6}\right] + \frac{1}{4\pi\epsilon_0}\sum_{i=1}^{3}\sum_{j=1}^{3}\frac{q_i q_i}{r_{ij}} \qquad (2.2)$$

in which ϵ_{io} and σ_{io} are the Lennard-Jones parameters for the interaction between the ion "i" and the oxygen atom "o" of a water molecule, while the Coulomb term incorporates the electrostatic interactions between the charges on the oxygen and hydrogen sites of a water molecule and the charge on an ion.

The molecular dipole moment of 2.35 D for SPC/E water is larger than the dipole moment of a free water molecule (1.86 D) but smaller than the estimated value for a water molecule in ice, which is 2.6 D. Guissani and Guillot[6] determined the liquid−vapor coexistence curve for this model by computer simulation and found the critical parameters ($T_c = 640$ K, $\rho_c = 0.29$ g cm^{-3}, and $P_c = 160$ bar) through a Wegner-type expansion for the order parameter along the coexistence curve. Except for the critical pressure, these values are in good agreement with the critical parameters for real water ($T_c = 647$ K, $\rho_c = 0.322$ g cm^{-3}, and $P_c = 221$ bar).[17a] The dielectric constant ϵ as a function of temperature for this model is also in accord with experiment, and the calculated values of $\epsilon = 81$ and ≈6 at 300 and 640 K agree with the measured 78 and 5.3, respectively.[17b]

The SPC/E model has been widely used over the past few years in computer simulation studies of the thermodynamic and transport properties of ions,[11,16] and the results are in good agreement with experimental properties at room temperature. In particular, the model succeeds in reproducing the actual

(12) Koneshan, S.; Rasaiah, J. C. *J. Chem. Phys.* 2000, 113, 8125.
(13) Rasaiah J. C.; Lynden-Bell, R. *Philos. Trans. R. Soc.*, to be published.
(14) Berendsen, H. J. C.; Grigera, J. R.; Straatsma, T. P. *J. Phys. Chem.* **1987**, *91*, 6269.
(15) (a) Dang, L. X. *Chem. Phys. Lett.* **1992**, *200*, 21. (b) Dang, L. X.; Garrett, B. C. *J. Chem. Phys.* **1993**, *99*, 2972. (c) Dang, L. X.; Kollmann, P. *J. Phys. Chem*. **1995**, *99*, 55. (d) Dang, L. X. *J. Am. Chem. Soc.* **1995**, *117*, 6954. (e) Dang, L. X. *J. Chem. Phys*. **1995**, *102*, 3483.
(16) Lynden-Bell, R. M.; Rasaiah, J. C. *J. Chem. Phys.* **1997**, *107*, 1981; **1996**, *105*, 9266.
(17) (a) Levelt Sengers, J. M. H.; Straub, J.; Watanabe, K.; Hill, P. G. *J. Phys. Chem. Ref. Data* **1985**, *14*, 193. (b) Mountain, R. D. *J. Chem. Phys.* **1999**, *110*, 2109.

dielectric constant, the thermodynamic properties, and the diffusion coefficient of water at 25 °C.[11] The atom pair correlation functions $g_{oo}(r)$, $g_{oh}(r)$, and $g_{hh}(r)$ are also in fair agreement with the neutron diffraction studies at 298 K.[18] For instance, a peak in the oxygen−hydrogen distribution functions $g_{oh}(r)$ at 1.8 Å, followed by a minimum at 3.3 Å, and a second peak at 4.5 Å, in the oxygen−oxygen distribution functions $g_{oo}(r)$, which is the signature of tetrahedral coordination, are observed in simulations of SPC/E water.

The SPC/E model has been used to model water far above room temperature, for which it had been originally designed. We have observed that the critical constants for this model are close to that of real water, and the dielectric constant in the supercritical region is small and similar to that for real water. We use the model extensively in our studies of ionic solutions in the supercritical region and assume that the implied constancy of the effective dipole moment of the molecule does not produce serious errors in our calculations. By using the same model potentials for water and ions at supercritical temperatures, we can directly compare our results with those under ambient conditions.

3. Method

The molecular dynamics simulations were carried out at constant NVT (canonical ensemble) using a time step of 1 fs. Each system was equilibrated for 500 ps before two (in some cases three) subsequent runs of 500 ps each were used in calculating ensemble averages. Specifically, the fifth-order Gear predictor−corrector algorithm was employed to integrate the equations of motion of the center of mass, and the quaternion method was used to solve the rotational equations of motion. The temperature was controlled as in previous work.[11,16] Following previous work, a reaction field was used to account for long-range Coulombic interactions:

$$u^{RF}(r_{ij}) = \frac{q_i q_i}{r_{ij}}\left\{\left(\frac{\epsilon_{RF}-1}{2\epsilon_{RF}+1}\right)\frac{r_{ij}^{\,3}}{R_c^{\,3}}\right\} \qquad (3.1)$$

Here, ϵ_{RF} is the dielectric constant surrounding the cutoff sphere of radius R_c, which is half the length of the simulation box. The values of ϵ_{RF} at 298.15 and 683 K were fixed at 22.0 and 5.0, respectively.

The simulation cell in the current study at 683 K was significantly larger than the cell that we had used under ambient conditions, because of the longer range in the correlations between particles near critical temperatures. The correlation length is given by[19]

$$\xi = \xi_0(\Delta T)^{-\nu}[1 + \xi_1(\Delta T)^{\Delta_1} + ...] \qquad (3.2)$$

where $\Delta T = (T - T_c)/T_c$, $\nu = 0.63$, and $\Delta_1 = 0.51$. For water, $\xi_0 = 1.3$ and $\xi_1 = 2.16$. At 683 K, the correlation length is 11 Å, which for a system of 216 water molecules at a density of 0.35 g cm^{-3} would be only slightly less than half the box length of nearly 13 Å. Increasing the number of solvent molecules to 511 increases the length of the simulation cell to 36 Å, to maintain the required density. This should be sufficient to prevent significant finite size errors in the calculated properties due to long-range critical correlations between the particles and is supported by our observations described below.

Increasing the size of the system to 512 particles has a negligible effect on the shape of the ion−oxygen and ion−hydrogen distribution functions, including such features as the location and height of the peaks in these functions. However, it significantly affected the partial molar volumes. It also had a non-negligible effect on both water−water and ion−water interaction energies. At 683 K, ion−water energy, with the reaction field correction discussed later, was approximately 6% more negative when 511 water molecules were used (∼ −58 kJ/mol) instead of 215. The difference between water−water Coulombic interaction in the pure water system of 511 molecules versus 511 water molecules plus Na^+ ion was about 2%, but it increased to 5% when the system size was reduced to 215 water molecules and the ion. On the other hand, the difference in the same property between pure water systems containing 511 1and 215 molecules was less than 1%. This implies that the introduction of an ion affects the average energy of the water−water interactions of the larger 511-molecule system far less than it does when the ion is introduced into the smaller 215-molecule system.

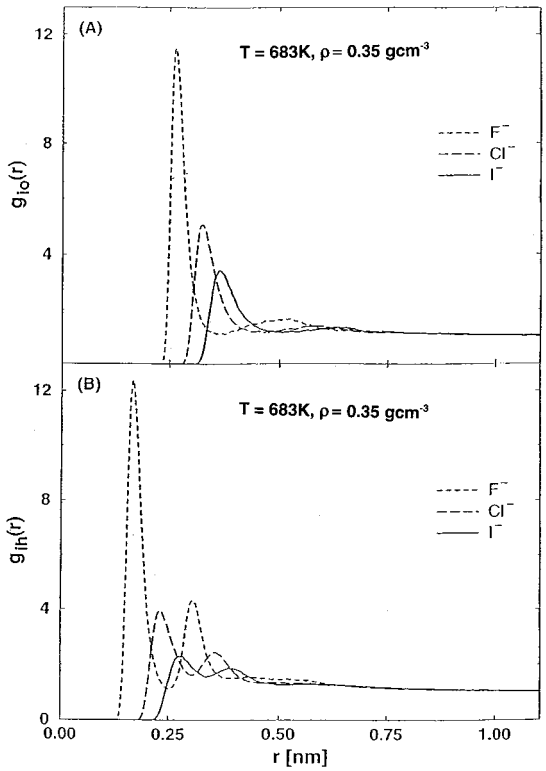

Figure 1. Ion−oxygen $g_{io}(r)$ (A) and ion−hydrogen $g_{ih}(r)$ (B) distribution functions for the anions F^-, Cl^-, and I^- at 683 K and solvent density of 0.35 g cm^{-3}.

The solutes used in this work fall into three categories—anions, cations, and uncharged particles which we call "drones". The primary set of systems in this study, at 683 K and a solvent density of 0.35 g cm^{-3}, consisted of the anions F^-, Cl^-, and I^-, the cations Li^+, Na^+, Rb^+, and Cs^+, and the fictitious ion I^+. The latter was identical to I^-, except for the reversed charge sign. Following previous work,[11] we also studied the uncharged solutes, Li°, Na°, Rb°, Cs°, and I°, by assigning zero charge to the corresponding ions. To investigate the effect of solvent density, some of the ions and "drones" in aqueous solution at solvent densities of 0.20 and 0.997 g cm^{-3} at 683 K were also studied.

4. Solvent Structure around the Solute

The time-averaged solvent structures around the solutes were investigated through calculations of the solute−solvent pair correlation functions. At room temperature (298 K) we observed a tall, sharp peak in g_{io} corresponding to the first solvation shell, followed by a shorter and broader second peak. The height of the peak decreased with the ion's diameter.[11] There was a significant difference between the ion−hydrogen distribution functions g_{ih} of negative and positive ions, which consisted of only one peak per hydration shell for cations, but two for anions.

The solute−solvent distribution functions at 683 K are sensitive to the solvent density. In Figures 1 and 2 we present the ion−oxygen and ion−hydrogen distribution functions $g_{io}(r)$ and $g_{ih}(r)$ at 683 K and a density of 0.35 g cm^{-3}, which is the primary system of interest in this work. The main features

(18) Soper, A. K.; Bruni, F.; Ricci, M. A. *J. Chem. Phys.* **1997**, *106*, 24712.

(19) Sengers, J. V.; Levelt Sengers, J. M. H. *Annu. Rev. Phys. Chem.* **1986**, *37*, 189.

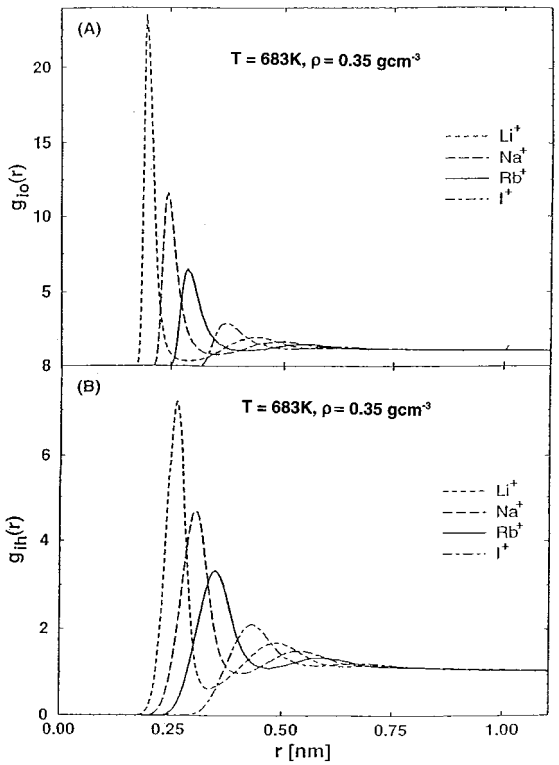

Figure 2. Ion−oxygen $g_{io}(r)$ (A) and ion−hydrogen $g_{ih}(r)$ (B) distribution functions for the cations Li^+, Na^+, Rb^+, and I^+ at 683 K and solvent density of 0.35 g cm^{-3}.

of the pair correlation functions under ambient conditions are preserved above the critical point. The peaks in ion−oxygen distribution functions g_{io} become shorter and broader with the increase of ion diameter, as shown in Figures 1 and 2.

The difference between these profiles at 683 and 298 K is in the relatively more diffused structure beyond the first solvation shell, regardless of the charge and size of an ion. As an example, we present here a comparison of g_{io} at different temperature/density conditions for Cl^- and Na^+ (Figures 3 and 4). The first peak in the ion−oxygen distribution function g_{io} occurs at about the same positions at 298 and 683 K, while the second peak, corresponding to the second hydration shell of the ion, is broader than its equivalent at room temperature. Moreover, it is not followed at 683 K by a clearly demarcated minimum separating it from the more remote region, indicating that the second solvation shell is qualitatively different in character from that at 298 K, probably due to increased rotational motion at high temperature. As in the earlier study at 298 K,[11] we observe a qualitative difference between the g_{ih} peaks for Cl^- and Na^+ ions at 683 K. For the negative chloride ion, the two peaks in the ion−hydrogen distribution function g_{ih} correspond to hydrogen atoms belonging to the same water molecule in the first solvation shell, with one hydrogen closer to the negative ion than the other. For the positive Na^+ ion, the two peaks in g_{ih} correspond to hydrogen atoms of distinct water molecules in the first and second hydration shells, respectively. This difference in the behavior of positive and negative ions toward the water in the primary hydration shell is due to the charge asymmetry of the SPC/E model for water. Details of the orientations of the water molecules in the hydration shells follow later in this section.

Table 2 shows that the peak heights of the distribution functions g_{io} and g_{ih} for all the ions at 683 K and a solvent density of 0.35 g cm^{-3} are higher than the corresponding values at 298 K and a solvent density of 0.997 g cm^{-3}. However, the

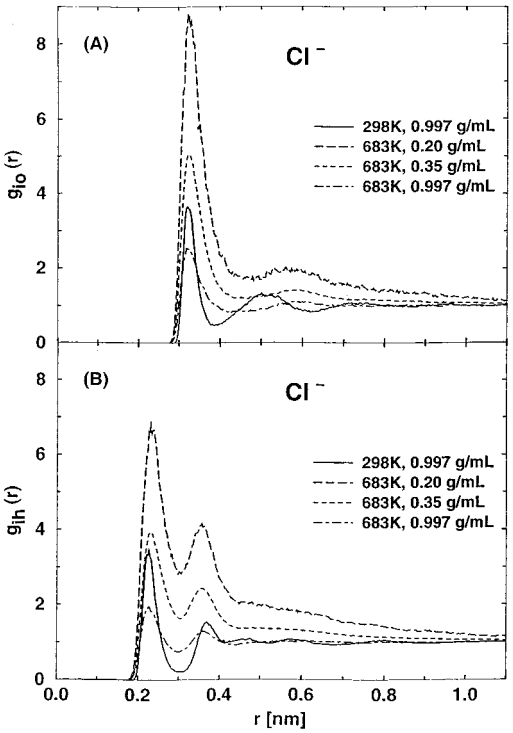

Figure 3. Comparison of g_{io} (A) and g_{ih} (B) under different temperature and density conditions. The solute is Cl^-.

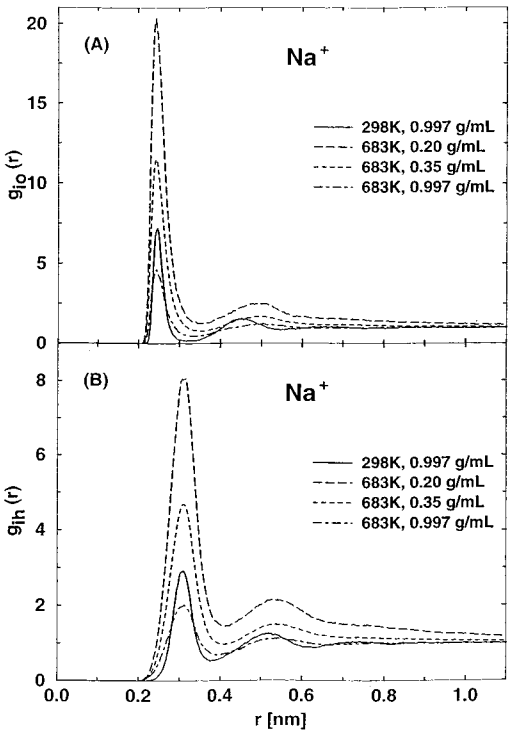

Figure 4. Comparison of g_{io} (A) and g_{ih} (B) under different temperature and density conditions. The solute is Na^+.

locations of the maximum and minimum (also shown in Table 2) in the solute−oxygen distribution functions for the first solvation shell are unchanged. The corresponding locations of these extrema for the second solvation shell are only slightly shifted toward larger distances (less than by 1 Å), compared to what is found under ambient conditions, for all of the solutes considered.

The detailed structure of the solvent around ions is affected by changes in solvent density. Table 2 also summarizes the

Table 2. Positions and Magnitudes at Maxima and Minima of Ion−Oxygen $g_{io}(r)$ Distribution Functions at 298 and 683 K

	298 K, 0.997 g cm^{-3}		683 K, 0.997 g cm^{-3}		683 K, 0.35 g cm^{-3}		683 K, 0.20 g cm^{-3}	
solute	r_{io} (Å)	g_{io}	r_{io} (Å)	g_{io}	r_{io} (Å)	g_{io}	r_{io} (Å)	g_{io}
				First Maximum				
F^-	2.6	7.9	2.6	4.6	2.6	11.0	–	–
Cl^-	3.2	4.1	3.2	2.6	3.2	5.0	3.2	8.8
I^-	3.6	2.7	3.6	2.0	3.6	3.4	–	–
Li^+	2.0	14.	2.0	7.8	2.0	23.0	–	–
Na^+	2.5	7.2	2.4	4.6	2.4	11.0	2.4	20.0
Rb^+	2.9	3.9	–	–	2.9	6.4	–	–
Cs^+	3.1	3.2	3.1	2.6	3.0	5.4	–	–
I^+	3.8	2.1	3.8	2.0	3.7	2.9	–	–
				First Minimum				
F^-	3.2	0.17	3.5	0.55	3.7	1.1	–	–
Cl^-	3.8	0.49	4.4	0.80	4.7	1.2	4.9	1.7
I^-	4.3	0.74	5.2	0.84	5.1	1.2	–	–
Li^+	2.7	0.02	2.9	0.26	2.9	0.32	–	–
Na^+	3.3	0.16	3.3	0.46	3.5	0.74	3.6	1.2
Rb^+	3.8	0.59	–	–	4.2	1.0	–	–
Cs^+	3.9	0.74	4.3	0.76	4.4	1.1	–	–
I^+	5.9	0.87	5.1	0.82	5.3	1.1	–	–
				Second Maximum				
F^-	4.5	1.5	5.1	1.1	5.3	1.7	–	–
Cl^-	5.0	1.3	5.9	1.1	5.8	1.4	5.6	2.0
I^-	5.1	1.3	6.6	1.1	6.3	1.4	–	–
Li^+	4.1	1.7	4.4	1.3	4.4	2.0	–	–
Na^+	4.5	1.4	5.0	1.2	4.9	1.7	4.9	2.5
Rb^+	5.1	1.1	–	–	5.6	1.5	–	–
Cs^+	5.4	1.1	5.9	1.1	5.8	1.4	–	–
I^+	none	none	6.8	1.1	6.3	1.3	–	–

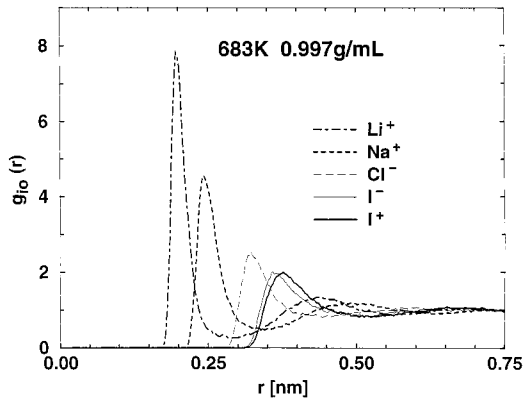

Figure 5. g_{io} correlation functions for various ions at 683 K and at the solvent density 0.997 g cm^{-3}.

positions and magnitudes of the maxima and minima in the distribution functions g_{io} and g_{ih} for several ions at 683 K and solvent densities of 0.997 and 0.20 g cm^{-3}. The positions of the first maximum and first minimum in g_{io} of Cl^- and Na^+ remain nearly the same, but the peak heights for each of these ions at 683 K increase with the decrease in solvent density. For example, the height of the first peak in the sodium−oxygen distribution function g_{io} at 683 K increases from 4.6 to 11 and then to 20 as the density decreases from 0.997 through 0.35 to 0.20 g cm^{-3}. Increasing the temperature from ambient to supercritical temperatures leads to a decrease in the peak heights, as shown in Figures 3 and 4. The general tendency of peaks in ion−oxygen distribution functions g_{io} to be lower and more diffuse with the increase of ion diameter remains unchanged at the three solvent densities studied (see Figure 5).

To gain further insight into the nature of the interactions that form the solvation shell, we also looked at the radial distribution

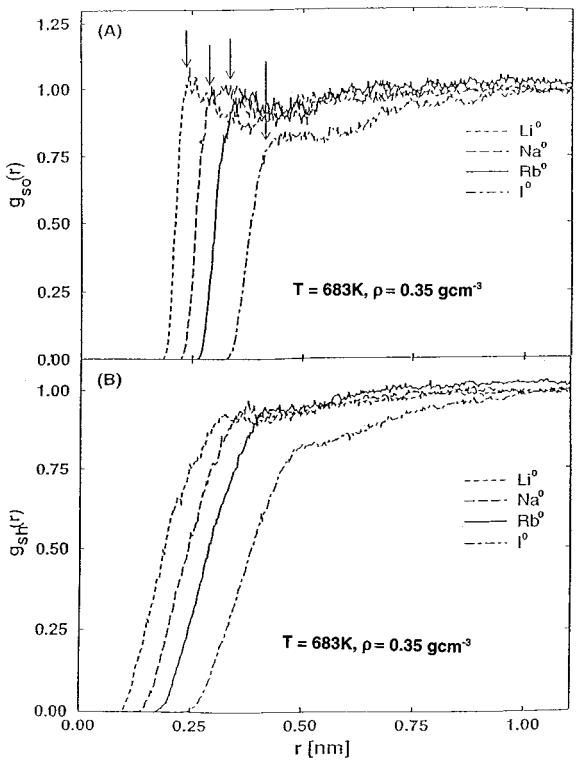

Figure 6. Solute−oxygen $g_{so}(r)$ (A) and solute−hydrogen $g_{sh}(r)$ (B) distribution functions for the uncharged solutes Li°, F°, Na°, Rb°, and I° at 683 K and solvent density of 0.35 g cm^{-3}. The arrows in (A) are at distances equal to the Lennard-Jones σ parameters for the solute−oxygen interactions.

functions of the water around the uncharged solutes. Unlike the results at room temperature,[11] characterized by prominent peaks in the solute−oxygen ("so") and solute−hydrogen ("sh") distribution functions, the corresponding distribution functions $g_{so}(r)$ and $g_{sh}(r)$ at 683 K and a solvent density of 0.35 g cm^{-3}, displayed in Figure 6, show no signs of significant hydrophobic solvation. Instead, the plots show a general depletion of solvent from the vicinity of the solute. This effect was noticed in the earlier studies of Guissani and Guillot[6] and Chialvo and Cummings.[7] Nevertheless, the solute−solvent distribution functions for the different uncharged solutes differ among themselves, with the smaller ones showing a small peak and the larger ones a short plateau followed by an asymptotic tail that eventually reaches unity. The sharp rise in the $g_{so}(r)$ distribution functions from zero shifts to larger distances as the size measured by σ_{io} increases. The differences in $g_{so}(r)$ of uncharged solutes beyond the initial sharp rise are small and are due to differences in their respective ϵ_{io} and σ_{io} parameters of the Lennard-Jones interaction.

The effects of solvent density on the solute−oxygen $g_{so}(r)$ and solute−hydrogen distribution functions $g_{sh}(r)$ of the uncharged Na° and I° are illustrated in Figures 7 and 8. Quite remarkably, increasing the solvent density to 0.997 g cm^{-3} restores hydrophobic solvation at 683 K. Visual inspection of the solvent configuration around the solute confirms cage formation, similar to what occurs at room temperature. These observations imply that hydrophobic solvation in the supercritical region of high compressibility should be sensitive to pressure changes that lead to changes in solvent density. The prominent solvation peak at 683 K at high density (0.997 g cm^{-3}) gradually disappears, as the density is decreased to 0.35 and to 0.20 g cm^{-3}, leaving no discernible first solvation shell.

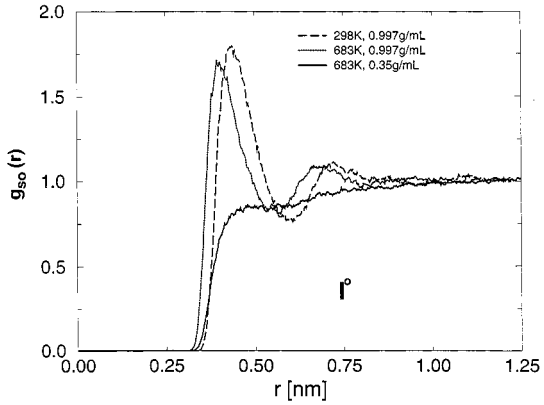

Figure 7. Comparison of solute−oxygen (A) and solute−hydrogen (B) distribution function for the uncharged I° under different temperature and density conditions.

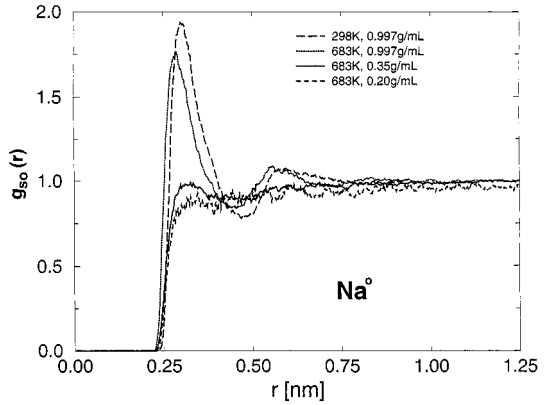

Figure 8. Comparison of solute−oxygen (A) and solute−hydrogen (B) distribution function for the uncharged Na° under different temperature and density conditions.

The distinction between positive and negative ions and uncharged species of the same size is clearest in studies of I^-, I^+, and I° because of its relatively large size that is kept the same for all three species. The only difference between the three is the charge. In Figure 9 we compare the respective solute−oxygen and solute−hydrogen distribution functions at 683 K at a solvent density of 0.35 g cm^{-3} with the corresponding values for these ions and uncharged species at 298 K and a solvent density of 0.997 g cm^{-3}. The location of the first maximum in $g_{io}(r)$ at 683 K is nearly identical for both ions I^+ and I^-, unlike the corresponding distribution functions at 298 K. The lack of structure around the uncharged species at high temperature and low solvent density can be attributed to the complete absence of cage formation due to reduced hydrogen bonding. As emphasized earlier, cage formation in the supercritical region is restored when the density is increased.

The hydration number N_h of the ions was calculated in the usual way as an integral of the ion−oxygen pair distribution function $g_{io}(r)$:

$$N_h = \rho_w \int_0^{R_h} g_{io}(r) 4\pi r^2 \, dr \qquad (4.1)$$

where R_h is the position of the first minimum in $g_{io}(r)$ and ρ_w is the density of water. The results are compared with the hydration numbers under ambient conditions[11] in Table 3. At a temperature of 683 K and solvent density of 0.20 g cm^{-3}, the only solutes studied were the chloride and sodium ions and the corresponding uncharged solutes Na° and Cl° obtained by turning off the charges on the ions. The "none" entries in the table for the hydration numbers of uncharged solutes at 683 K reflect the absence of hydration.

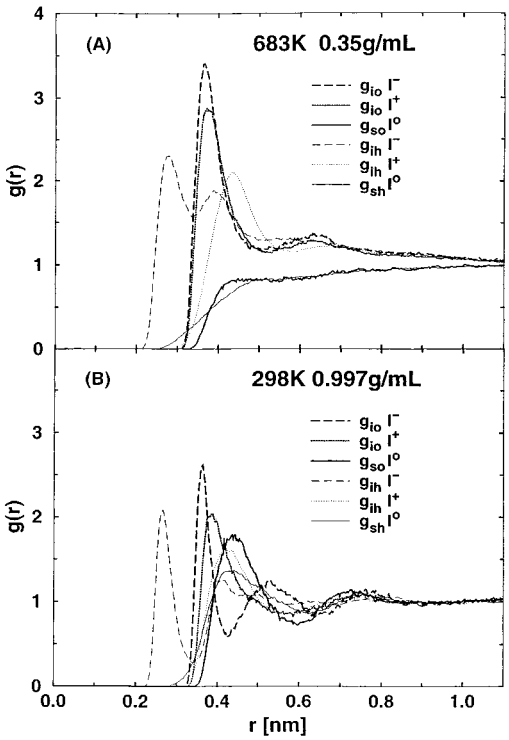

Figure 9. Comparison of the solute−oxygen and solute−hydrogen distribution functions for I°, I^-, and I^+ at 683 (A) and 298 K (B).

Table 3. Coordination Numbers of Water in First Hydration Shells of Solutes under Ambient and Supercritical Conditions[a]

	hydration numbers			
solute	298K, 0.997 g cm^{-3}	683 K, 0.997 g cm^{-3}	683 K, 0.35 g cm^{-3}	683 K, 0.20 g cm^{-3}
F^-	6	7	6	−
Cl^-	7	10	8	7
I^-	8	17	9	−
Li°	11	8	none	−
Na°	13	12	none	none
F°	17	15	none	−
Cl°	23	19	none	none
I°	27	22	none	−
Li^+	4	5	4	−
Na^+	6	6	5	5
Rb^+	8	−	6	−
Cs^+	8	11	7	−
I^+	25	17	9	−

[a] The absence of an entry, denoted by (−) in this table, means no simulations were carried out for that state variable.

Hydrophobic solvation of the uncharged solutes ("drones) at 298 K is due to cage formation, in which the water molecules making up the cage are held together by hydrogen bonds. The size of the cage is reflected in the hydration numbers of the "drones", which increase monotonically with the size of the solute. The cage around an uncharged solute tends to collapse at supercritical temperatures. Applying pressure to increase the solvent density can reverse this effect. The solvent is, of course, highly compressible in the supercritical region. For example, Table 3 shows that the "drones" lack hydration shells at 683 K and a solvent density of 0.35 g cm^{-3} but regain the shells when the density is raised to 0.997 g cm^{-3}. The hydration number at this density increases with the size of the uncharged solute, as it does at 298 K.

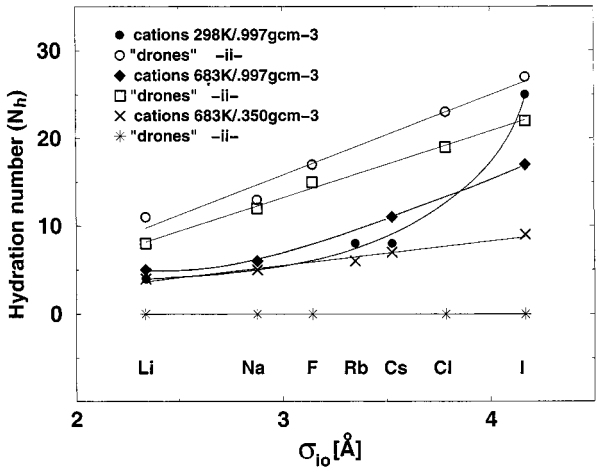

Figure 10. Comparison of the hydration numbers of cations and anions as a function of their size σ_{io} at 683 and 298 K.

In general, the changes in the hydration numbers with temperature are minor for small ions and more substantial for larger ones. Among the charged species, the most dramatic changes in the hydration numbers with temperature and density occur for the large I^+ and I^- ions, as seen in Figure 10. There, we plot the hydration number N_h vs σ_{io}, where σ_{io} is the Lennard-Jones parameter for uncharged solutes and ions given in Table 1. The dependence is nearly linear at both temperatures, except for the cation of iodine I^+, which shows strong positive deviation under ambient conditions due to hydrophobic solvation, discussed also in previous work.[11,16] Quite remarkably, the slopes at 683 and 298 K are also nearly identical, except for the deviations observed for the large ions I^+ and I^-.

In previous studies,[11] it was shown that the asymmetric charge distribution of the water molecule determines the orientation of water in the first hydration shell of cations and anions. The average orientation of water near a solute depends strongly on the sign of the solute charge. Similar trends are equally valid under supercritical conditions. The first peak in the ion−oxygen distribution function $g_{io}(r)$ at 683 K is sharp for small ions and broader for larger ions. For cations, the first peak in the cation−hydrogen distribution function follows the first peak in the ion−oxygen distribution function. The former comes mainly from the hydrogen of the same water molecule that contributes to the first peak in $g_{io}(r)$. This fact clearly corresponds to an orientation in which the symmetry axis of the water molecule is, on average, in the same plane as the cation−oxygen vector, with the oppositely charged oxygen and cation facing each other, forcing the hydrogen of the water outward. For anions, the first ion−oxygen peak in $g_{io}(r)$ is sandwiched between two ion−hydrogen peaks in the $g_{ih}(r)$ correlation functions that belong to the same water molecule. This is seen clearly by comparing Figure 1A and B; the distance between the first peaks in $g_{ih}(r)$ and $g_{io}(r)$ functions for anions is nearly equal to the OH distance in a water molecule. The second hydrogen peak of $g_{ih}(r)$ and the oxygen peak of $g_{io}(r)$ overlap significantly. The implied orientation of the water molecule has one of the hydrogens pointed toward the anion, with the water dipole at approximately 40−50° to the line connecting the anion with the oxygen. This qualitative difference between the hydration of positive and negative ions is, of course, absent in a continuum model, and also in simple dipolar or tetrahedral molecular models for water.

These conclusions are confirmed by our calculations of the time-averaged probability distributions $\langle P_\theta \rangle$ and $\langle P_\phi \rangle$ of the orientations of water molecules in the first hydration shell. Here,

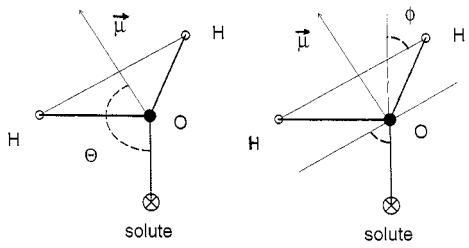

Figure 11. Angles θ and ϕ defining the orientation of a water molecule in the vicinity of a solute.

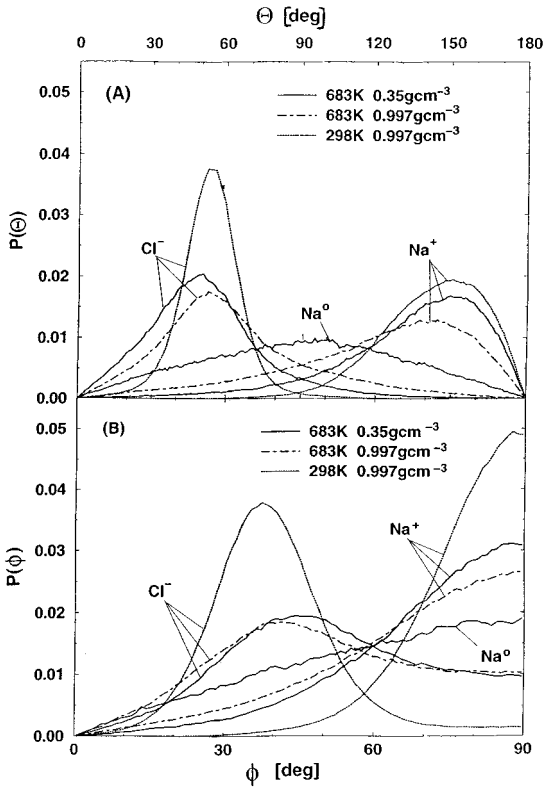

Figure 12. Comparison of orientation of water in the first hydration shell of Cl^-, Na^+, and Na° under different temperature/density conditions. Orientations are given in terms of θ (A) and ϕ (B).

θ is the angle between the water dipole and the line joining the water oxygen to the solute, and ϕ is the acute angle between the line joining the oxygen to the solute and the line joining the hydrogen atoms of the same water molecule, as illustrated in Figure 11.

In Figure 12, plots of $\langle P_\theta \rangle$ and $\langle P_\phi \rangle$ are presented for water in the first hydration shells of Cl^-, Na^+, and uncharged Na° at different temperature/density conditions. For the "drone" Na°, the plots of of $\langle P_\theta \rangle$ and $\langle P_\phi \rangle$ are nearly identical, regardless of temperature and density. Figure 13 presents the corresponding plots for the iodine solutes I^+, I^-, and I°. The most probable values of $\langle \theta \rangle$ and $\langle \phi \rangle$ for the species studied, corresponding to the maxima in the distribution functions, are given in Table 4. The tables confirm that the orientations of water in the first hydration shell are different for cations and anions, as expected from the charge asymmetry of the water molecule. For cations, the negatively charged oxygen atom of the water of hydration is closer to the ion than the symmetrically disposed positively charged hydrogen atoms of the same water molecule. The dipole moment of the hydrating water is tilted away from the line joining the ion to the oxygen atom. The angle of tilt increases with the size of the cation. When the ion is negatively charged,

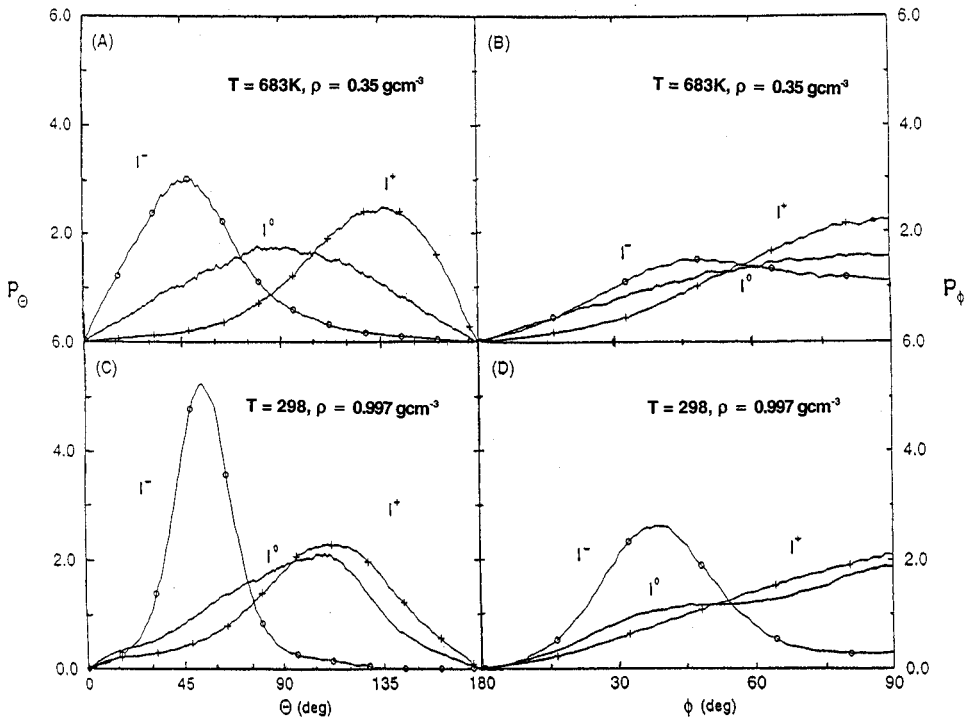

Figure 13. Plots of $P(\theta)$ vs θ and $P(\phi)$ vs ϕ at 683 K and solvent density 0.35 g cm^{-3} (A, B) and at 298 K and solvent density of 0.997 g cm^{-3} (C, D) for iodine solutes. θ is the angle between the water dipole and the line joining the solute and the oxygen of water in the first hydration shell. ϕ is the angle between the lines solute−oxygen and hydrogen−hydrogen. Probabilities of finding the configuration at a given angle, P_α, are normalized to the corresponding bulk solution values.

Table 4. Orientation of Water Molecules in the First Hydration Shells around Solutes at Room Temperature and under Supercritical Conditions

	Θ (deg)		ϕ (deg)	
solute	298 K, 0.997 g cm^{-3}	683 K, 0.35 g cm^{-3}	298 K, 0.997 g cm^{-3}	683 K, 0.35 g cm^{-3}
F^-	53	52	37	40
Cl^-	53	50	38	44
I^-	52	45	38	45
Li°	100	−	90	−
Na°	103	98[a]	90	90[a]
I°	113	90[a]	90	90[a]
Li^+	165	160	90	90
Na^+	150	150	90	90
Rb^+	−	148	−	90
Cs^+	129	147	90	90
I^+	113	137	90	90

[a] For this result, the center of the plateau in g_{io} has been used in place of the first minimum in g_{io} to locate the boundary of the first shell.

one hydrogen atom belonging to the hydrating water is closer to the ion than the other hydrogen of the same molecule, leading to two distinct peaks in the ion−hydrogen distribution functions, as pointed out earlier (see Figures 1 and 2). The anion and the OH bond of the hydrogen that is closest to it are nearly collinear. It follows from simple geometry and the fact that the HOH angle in water is ≈105° that θ and ϕ are nearly 53° and 38°, respectively, for anions, as shown in Table 4.

For the uncharged species at 298 K, $\theta \approx 100°$, and the water dipoles are within 10° of being perpendicular to the line joining the solute to the oxygen. This orientation favors cage formation around the solute, in which the water molecules are held together by hydrogen bonds. The cages break down at 683 K when the solvent density is 0.35 g cm^{-3} but reappear at a higher density of 0.997 g cm^{-3} at this temperature. This shows how structure is altered by changes in the solvent density by applying pressure. At the lower densities, the water molecules in the vicinity of the uncharged solute at 683 K have a broader distribution of orientations, as seen in Figures 11 and 12. However, there is still a small preference for the water dipoles to be perpendicular to the line joining the solute to the oxygen.

Although the equilibrium positions of the water molecules in the first solvation shell of the ions at 298 K are essentially unchanged by changes in temperature or solvent density, it does not exclude the possibility that the residence times and dynamics of the hydration shells may be significantly altered. The residence times of water in the primary shells are discussed in the following paper, together with other dynamical properties of these systems.[33]

5. Partial Molar Volumes of Solutes

The solvation of ions under supercritical conditions has been studied previously by Chialvo and Cummings.[7] The same authors also looked at the small, nonpolar particles in infinitely dilute aqueous solution. For He and Ne atoms, they found positive values of the partial molar volume and the same characteristic lack of a solvation shell around the solutes at low solvent density (<0.35 g cm^{-3}) presented here for uncharged species.

The divergence of the partial molar volume of a solute, $\overline{V_2^\infty}$, near the critical temperature is well known and is associated with the divergence of the solvent compressibility. We calculate the partial molar volume from the angularly averaged pair distribution functions g_{iw} and g_{ww}, where indices "i" and "w" stand for the solute and the center of mass of water molecule, respectively. It follows from the Kirkwood−Buff theory[20] of solutions in the limit of zero solute number density ($\rho_2 \rightarrow 0$) that

(20) Kirkwood, J.; Buff, R. P. *J. Chem. Phys.* **1951**, *19*, 774.

$$\overline{V_2^{\infty}} = \frac{1}{\rho_1} + G_{11}^{\circ} - G_{12}^{\infty} = kT\kappa_T - G_{12}^{\infty} \qquad (5.1)$$

The subscripts 1 and 2 refer to the solvent and the solute, respectively, and the superscripts ° and ∞ denote the pure solvent and infinitely dilute solution, respectively. κ_T is the isothermal compressibility of the pure solvent, and ρ_1 is the solvent number density. Additionally, the G_{ij} functions in eq 5.1 are defined in terms of $h_{ij}(r) = g_{ij}(r) - 1$ by the relation

$$G_{ij} = \frac{1}{\Omega}\int_0^{\infty} h_{ij}(\mathbf{r})\, d\mathbf{r} = \tilde{h}_{ij}(0) \qquad (5.2)$$

Here, $g_{ij}(r)$ is the solute−solvent pair correlation function, and $\Omega = 4\pi$ or $8\pi^2$, depending on whether the solvent is a linear or nonlinear molecule. The solute is assumed to be spherically symmetric, and $\tilde{h}_{ij}$ is the $k \rightarrow 0$ limit of the Fourier transform of this function, defined by

$$\tilde{h}_{ij}(k) = \frac{1}{\Omega}\int_0^{\infty} h_{ij}(\mathbf{r}) \exp(i\mathbf{k}\cdot\mathbf{r})\, d\mathbf{r} \qquad (5.3)$$

The isothermal compressibility κ_T of the pure solvent is related to G_{11}° by

$$\rho_1 kT\kappa_T = 1 + \rho_1 G_{11}^{\circ} \qquad (5.4)$$

We used eq 5.1 to calculate the partial molar volumes, with the correlation length chosen as an integration limit in eq 5.2 for the supercritical data with 511 particles. At room temperature, the systems were smaller (215 instead of 511 solvent molecules), and the integration limit was ≈8 Å, beyond which the radial distribution functions showed no oscillations regardless of the particular choice of solute. From eq 5.4 we evaluate the isothermal compressibility of the solvent at a density of 0.32 g cm^{-3} and a temperature of 683 K. The result, expressed as $kT\kappa_T$, is estimated to be 130 cm^3/mol.

The results of our calculations of the partial molar volumes for all the systems investigated in this work at 683 K, and a representative choice of data at room temperature, are shown in Table 5. Note the order of magnitudes and signs of the partial molar volumes at the two different temperatures. They are large and negative for all the ions at 683 K, in contrast to the large positive values for the uncharged species at this temperature.

As Figure 14 shows, at 683 K the partial molar volumes of cations and anions are negative and show a weak dependence on solute size. For uncharged solutes, the partial molar volumes are positive at 683 K, and the dependence on size is linear with values in the range of 200−500 cm^3/mol. This is different from the behavior in ambient solutions, where the sign of the partial molar volume of the ion depends on the ion size. The most prominent change occurs for anions (Figure 14B), for which the negative sign of $\overline{V_2^{\infty}}$ for the small ion F^- becomes positive for larger ions, e.g., Cl^- and I^-.

We have noted that the partial molar volumes of the ions and uncharged solutes are of opposite sign at 683 K. The compressibility diverges as the critical temperature is approached, which is mirrored by the large magnitudes of partial molar volumes of the solutes. The reason for this, and for the sign difference in the partial molar volumes of ions and uncharged solutes in the supercritical region, is seen more clearly

Table 5. Partial Molar Volume of Solutes at 298 and 683 K

	$\overline{V_2^{\infty}}$ (cm^3 mol^{-1})		$\overline{V_2^{\infty}}/(kT\kappa_T)^a$ 683 K, 0.35 g cm^{-3}	
solute	298 K, 0.997 g cm^{-3}	683 K, 0.35 g cm^{-3}	simulation	calculation
Li°	6	213	1.6	1.6
Na°	14	252	1.9	2.1
F°	−	313	2.4	2.4
Rb°	−	323	2.5	2.7
Cl°	−	350	2.7	3.5
I°	50	431	3.3	4.3
Li^+	−8	−431	−3.31	−
Na^+	−10	−457	−3.51	−
Rb^+	−	−406	−3.12	−
Cs^+	19	−413	−3.18	−
I^+	43	−280	−2.15	−
F^-	−19	−601	−4.62	−
Cl^-	15	−428	−3.29	−
I^-	26	−337	−2.59	−

[a] $kT\kappa_T$(693 K) = 130 cm^3/mol.

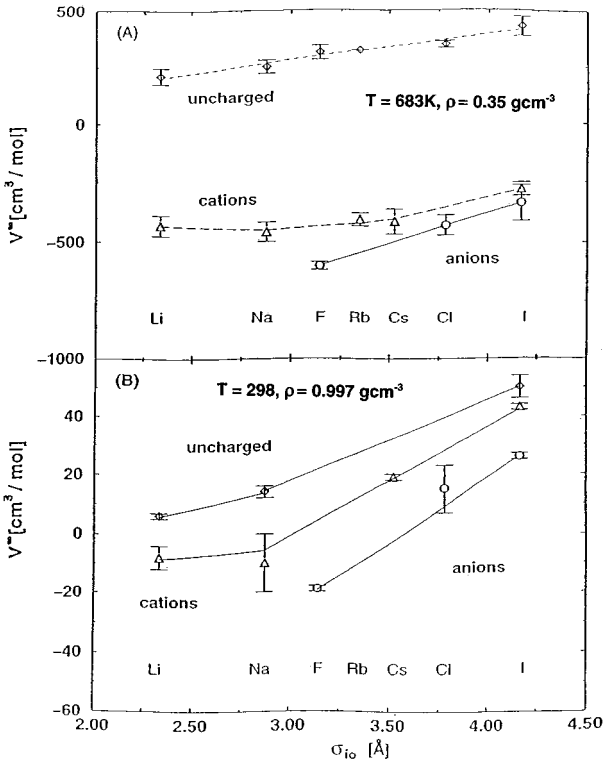

Figure 14. Partial molar volumes of ions and uncharged solutes as a function of size at 683 K and a solvent density of 0.35 g cm^{-3} (A) and at 298 K and a solvent density of 0.997 g cm^{-3} (B).

by expressing $\overline{V_2^{\infty}}$ in terms of the integral of the direct correlation function, which is

$$C_{12}^{\infty} = \frac{1}{\Omega}\int_0^{\infty} c_{12}^{\infty}(\mathbf{r})\, d\mathbf{r} \qquad (5.5)$$

It follows from the Ornstein−Zernike equation in Fourier space in the limit $\rho_2 \rightarrow 0$ that

$$\tilde{h}_{12}^{\infty}(k) = \tilde{c}_{12}^{\infty}(k) + \rho_1 \tilde{h}_{11}^{\circ}(k)\tilde{c}_{12}^{\infty}(k) \qquad (5.6)$$

which is equivalent to

$$\tilde{c}_{12}^{\infty}(k) = \frac{\tilde{h}_{12}^{\infty}(k)}{1 + \rho_1 \tilde{h}_{11}^{\circ}(k)} \qquad (5.7)$$

In the limit $k \rightarrow 0$, it follows from eqs 5.4 and 5.6 that

$$G_{12}^{\infty} = kT\kappa_T\rho_1 C_{12}^{\infty} \tag{5.8}$$

Combining this with eq 5.1, we see that

$$\overline{V_2^{\infty}} = kT\kappa_T[1 - \rho_1 C_{12}^{\infty}] \tag{5.9}$$

This is the product of two factors. The first of these, $kT\kappa_T$, is determined by the properties of the pure solvent and diverges at the critical point along with the compressibility κ_T. Since the compressibility $\kappa_T > 0$, the positive or negative sign of the partial molar volume $\overline{V_2^{\infty}}$ is determined by the sign of the second factor $(1 - \rho_1 C_{12}^{\infty})$. This depends primarily on the solute−solvent interactions. Equation 5.9 was discussed earlier by Brelvi and O'Connell[21] and is widely quoted in the chemical engineering literature.[1,22]

Chang, Morrison, and Levelt Sengers[23] showed that the factorization of the partial molar volume of a solute of mole fraction x follows from the thermodynamic identities

$$\overline{V_2} = V + (1 - x)(\partial V/\partial x)_{PT} \tag{5.10}$$

$$(\partial V/\partial x)_{PT} = V\kappa_{T,x}(\partial V/\partial x)_{VT}$$

Here, $\kappa_{T,x}$ is the isothermal compressibility at constant composition and $(\partial P/\partial x)_{VT}$ is called the Krichevskii parameter,[1b] which is related to the factor in square brackets in eq 5.9. Chang, Morrison, and Levelt Sengers[23] pointed out that the partial molar volume of the solute at infinite dilution near the solvent critical point is path dependent. If the limit $x \rightarrow 0$ is taken first, $\kappa_{T,x}$ becomes the isothermal compressibility of the pure solvent and diverges as $|T - T_c|^{-\gamma}$, with the critical exponent γ equal to 1 for classical and 1.24 for nonclassical behavior. If the limit $x \rightarrow 0$ is not taken first, there are two or three modes of approach to the critical point, depending on whether one assumes classical or nonclassical behavior. Our simulations at 683 K are nearly 30−40 degrees away from the critical temperature, where these distinctions are of no special relevance, and the partial molar volume is uniquely defined.

The angularly averaged solute−solvent correlation functions $c_{12}(r)$ and $h_{12}(r)$ are nearly the same as the solute−oxygen $c_{io}(r)$ and $h_{io}(r)$, respectively, if we ignore the effect due to the displacement of the center of mass of the water molecule from the position of the oxygen atom. Likewise, the angularly averaged solvent−solvent correlation function $h_{11}(r)$ is essentially $h_{oo}(r)$. With these assumptions, we can calculate $c_{io}(r)$ from our simulation data for $g_{io}(r)$ or $g_{so}(r)$ and $g_{oo}(r)$ by using eq 5.7 and numerical Fourier transformations. The correlation functions $c_{io}(r)$ for Na^+ and $c_{so}(r)$ Na° at 683 K and a solvent density of 0.35 g cm^{-3} calculated in this way are compared in Figure 15A and B with the corresponding total correlation functions $h_{io}(r)$ and $h_{so}(r)$. The figures highlight the similarities and differences between the two functions at different values of the ion−oxygen distance r. The direct correlation function $c_{io}(r)$ or $c_{so}(r)$ is much simpler than the corresponding total correlation functions $h_{io}(r)$ and $h_{so}(r)$, and therefore easier to approximate.

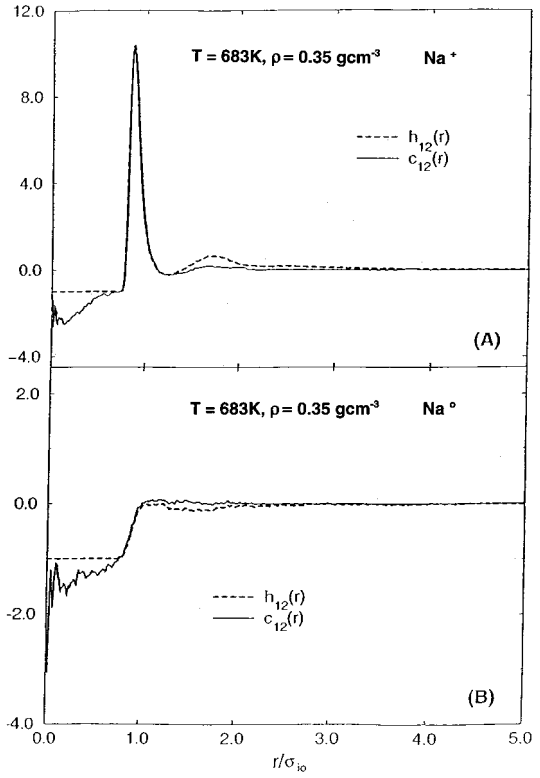

Figure 15. Comparison of the direct and indirect solute−oxygen correlation functions $c_{io}(r)$ or $c_{so}(r)$ and $h_{io}(r)$ or $h_{so}(r)$ respectively for Na^+ (A) and Na° (B) at 683 K and 0.35 g cm^{-3}. In the figure, these functions are labeled $c_{12}(r)$ and $h_{12}(r)$, respectively.

In an infinitely dilute solution of an uncharged solute, away from the critical point, the integral of solute−solvent direct correlation function $c_{12}(r)$ can be approximated by the integral of the Mayer f-function,

$$f_{12}(r,\omega) = \exp[-\beta u_{12}(r,\omega) - 1] \tag{5.11}$$

where $\beta = 1/kT$ and $u_{12}(r,\omega)$ is the corresponding solute−solvent pair potential. Inserting this in eq 5.5, we see that integral C_{12}^{∞} is related to the second virial coefficient $B_{12}(T)$ for this potential, and

$$\overline{V_2^{\infty}} = kT\kappa_T[1 + 2\rho_1 B_{12}(T)] \tag{5.12}$$

where

$$B_{12}(T) = \frac{1}{2\Omega}\int\int\int f(r,\omega)r^2\,dr\,\sin\theta\,d\theta\,d\varphi \tag{5.13}$$

This is a simple approximation for the partial molar volume of a solute at infinite dilution. The ratio of the partial molar volumes of two uncharged solutes is equal to the ratio of the quantity in square brackets in eq 5.12 or, more accurately, in eq 5.9. Equation 5.12 has been suggested earlier[24] and is discussed in the chemical engineering literature. At higher solvent densities, integral equation approximations for the

(21) (a) Brelvi, S. W.; O'Connell, J. P. *AIChE J.* **1972**, *18*, 1239. (b) O'Connell, J. P. *Fluid Phase Equil.* **1981**, *6*, 21 (c) O'Connell, J. P. Thermodynamics and Fluctuation Solution Theory with Some Applications to Systems at or Near Supercritical Conditions. In *Supercritical Fluids Fundamentals and Applications*; Kiran, E., Levelt Sengers, J. M. H., Eds.; NATO ASI Series 271; Kluwer Academic Publishers: Dordrecht, The Netherlands, 1994.

(22) (a) Petsche, I.; Debenedetti, P. G. *J. Phys. Chem.* **1991**, *95*, 386. (b) Abdulagatov, I. M.; Bazaev, A. R.; Bazaev, E. A.; Saidakhmedova, B.; Ramazanova, A. E. Presented at the Thirteenth Symposium on the Thermophysical Properties, June 1997, Boulder, Colorado.

(23) Chang R. F.; Morrison G.; Levelt Sengers, J. M. H. *J. Phys. Chem.* **1984**, *88*, 3389.

(24) O'Connell J. P.; Sharygin, A. V.; Wood, R. H. *Ind. Eng. Chem. Res.* **1996**, *35*, 2808.

solute−solvent direct correlation function should provide a better estimate of the factor in square brackets in eq 5.9.

The solute−solvent potential in our model has a Lennard-Jones form, and $B_{12}^{LJ}(T)$ is available from tables[25] or can be calculated numerically in the reduced form

$$B_{12}^{LJ,*}(T^*) = -2\pi \int_0^\infty \exp[-(4/T^*)(r^{*-12} - r^{*-6})] r^{*2}\, dr^* \tag{5.14}$$

where $r^* = r/\sigma_{io}^3$. It follows that the partial molar volume of an uncharged solute interacting with the solvent through a Lennard-Jones potential is given by

$$\overline{V_2^\infty} = kT\kappa_T[1 + 2\rho_1^* B_{12}^{LJ,*}(T^*)] \tag{5.15}$$

where the reduced density of the solvent $\rho_1^* = \rho_1\sigma_{io}^3$ and $V_2^\infty/kT\kappa_T$ obeys a law of corresponding states. At high temperatures, the Mayer *f*-function for the Lennard-Jones interaction between the solute and solvent is essentially a step for the repulsive core of the potential, and $B_{12}^{LJ}(T) \approx 2\pi\sigma_{io}^3/3$. The partial molar volumes of uncharged solutes, using this approximation for the second virial coefficient and the solvent compressibility determined from our simulations of the solvent correlation functions through eq 5.4, are displayed in Table 5. Although eq 5.15 is expected to hold only at low solvent density, our calculations at 683 K and a solvent density 0.35 g cm^{-3} show that it is fairly accurate, especially for smaller uncharged solutes.

A solvent density of 0.35 g cm^{-3} corresponds in our case to a reduced density $\rho_1\sigma_{oo}^3 \approx 0.34$, which is rather high for the second virial coefficient approximation to be considered adequate. Indeed, Harvey[26] showed that the second virial coefficient approximation is inadequate for calculations of the partial molar volumes in the supercritical region. To explore this further, we calculated $[1 - \rho_1 C_{12}^\infty]$ from the Percus−Yevick approximation for a hard-sphere binary mixture,[27] in the limit of zero solute density, treating the solvent correlation as also due to hard spheres. This approximation automatically includes the dominant contributions of the higher virial coefficients of hard spheres but treats the correlation between the solvent water molecules as that between hard spheres, which is clearly an approximation. The agreement with our simulations is worse; it leads to values of $[1 - \rho_1 C_{12}^\infty]$ that are larger than the corresponding estimates from the hard-sphere second virial coefficients B_{12}^{HS} by factors ranging from 1.3 for Li° to 2.5 for I°. The good agreement displayed in Table 5 may be due to a cancellation of errors. This arises from treating the Lennard-Jones interactions as hard spheres, in the second virial coefficient approximation, and the neglect of higher virial coefficients for the true interaction between the uncharged solute and the solvent, as well as that between solvent molecules. The attractive well in the Lennard-Jones interaction will produce contributions of sign opposite to those of the contributions of the higher virial coefficients that are neglected in the approximation for $[1 - \rho_1 C_{12}^\infty]$ that is used, thereby partly canceling their effect.

Equation 5.12 can also be used to discuss qualitatively the partial molar volumes of ions at infinite dilution. Treating the water molecule, for this purpose, as a simple dipole, the ion solvent interaction

$$u_{12}(r,\omega) = u_{12}^{LJ}(r) + u_{12}^{CD}(r,\omega) \tag{5.16}$$

is the sum of Lennard-Jones and charge dipole terms and the Mayer *f*-function is given by

$$f_{12}(r,\omega) = [1 + f_{12}^{LJ}(r)] \exp[-\beta u_{12}^{CD}(r,\omega) - 1]$$
$$= f_{12}^{LJ}(r) + [1 + f_{12}^{LJ}(r)] \sum_{n=1}^{\infty} \frac{(-1)^n}{n!} (\beta u_{12}^{CD}(r,\omega))^n \tag{5.17}$$

Substituting this in the expression for the second virial coefficient, we find

$$B_{12}(T) = B_{12}^{LJ}(T) - \frac{1}{2\Omega} \int\int (1 + f_{12}^{LJ}(r)) \sum_{n=1}^{\infty} (-1)^n \frac{(\beta u_{12}^{CD})^n}{n!} r^2\, dr\, d\vec{\omega} \tag{5.18}$$

where $d\vec{\omega} = \sin\theta\, d\theta\, d\phi$. The charge dipole potential $u_{12}^{CD}(r,\omega)$ is given by the relation

$$u_{12}^{CD}(r,\omega) = -\frac{q\mu}{r^2}\cos\theta \tag{5.19}$$

Here, μ is the dipole moment of the solvent and θ is the angle between the dipole moment vector and the line joining the centers of mass of the ion and the dipolar solvent. Using this in the expression for $B_{12}(T)$, we see that all the odd terms in the summation vanish on angular integration, and only even terms survive. This is fortunate, as the spatial integral of the $n = 1$ term diverges. It follows that

$$B_{12}(T) = B_{12}^{LJ}(T) - \frac{1}{2\Omega} \int\int (1 + f_{12}^{LJ}(r)) \sum_{n=2,4,6\ldots} \frac{(\beta q\mu)^n}{n! r^{2n}} r^2\, dr \cos^n\theta\, d\vec{\omega}$$
$$= B_{12}^{LJ}(T) - \frac{1}{2} \int (1 + f_{12}^{LJ}(r)) \sum_{n=2,4,6\ldots} \frac{(\beta q\mu)^n}{n!(n+1) r^{2n-2}}\, dr \tag{5.20}$$

This can be evaluated numerically or analytically by expanding the exponential term in the Mayer *f*-function. At supercritical temperatures, $f_{12}^{LJ}(T)$ can be approximated by the Mayer *f*-function for hard spheres of diameter σ_{io}, which is a unit step function. Spatial integration then leads to

$$B_{12}(T) \approx \left[\frac{2\pi}{3} - \sum_{n=2,4,6\ldots} \frac{1}{n!(n+1)(2n-3)} \left(\frac{\beta q\mu}{\sigma_{io}^2}\right)^n\right] \sigma_{io}^3 \tag{5.21}$$

The charge appears as an even power in this expression, which is therefore independent of the sign of the charge. $B_{12}(T)$ changes from positive to negative values as the charge on the ion or dipole moment μ of the solvent increases from zero. This implies that the partial molar volume of the solute changes sign as $2\rho_1 B_{12}(T)$ varies from values greater than to less than -1; it is zero in this approximation when $2\rho_1 B_{12}(T) = -1$. The exact condition for zero partial molar volume is $\rho_1 C_{12}^\infty(T) = 1$, as seen from eq 5.9. This condition depends on the temperature, the ion size and charge, and the magnitude of the dipole moment of the solvent. The conditions leading to this state are

(25) Hirschfelder, J. O.; Curtiss, C. F.; Bird, R. B. *Molecular Theory of Gases and Liquids*; John Wiley: New York, 1954.
(26) Harvey, A. H. *Fluid Phase Equil.* **1997**, *130*, 87.
(27) Isbister, D. *Mol Phys* **1976**, *32*, 949.

experimentally accessible, and zero partial molar volume should be observable in the laboratory. The second virial coefficient approximation for the partial molar volume of ions should be more accurate when ($\beta q\mu/\sigma_{io}^2$) is small, e.g., for a large ion such as the $(CH_3)_4N^+$ ion under conditions of temperature and solvent dipole moment that make this parameter small.

5. Summary and Conclusions

We have carried out molecular dynamics studies of the structures of an extensive set of positive, negative, and uncharged solutes at infinite dilution under supercritical conditions of 683 K and a solvent density of 0.35 g cm^{-3}. Simulations of a less extensive set of ions and "drones" at solvent densities of 0.997 g cm^{-3} and 0.20 g cm^{-3} at 683 K were also performed. Our studies include calculations of the ion−oxygen and ion−hydrogen distribution functions, the coordination numbers at 683 K, and the partial molar volumes of the ions and uncharged solutes at infinite dilution at 683 and 298 K.

The hydration numbers of uncharged solutes, or "drones", reflect the extent and size of the hydrogen-bonded cages around the solutes. The cages tend to break down in the supercritical region studied (∼683 K) at low solvent density (<0.35 g cm^{-3}) but can be restored by applying pressure to increase the solvent density to near 0.997 g cm^{-3}. Small cations and anions have essentially the same hydration numbers at 298 and 683 K, while the hydration of the large anion I^- and the fictitious ion I^+ at 683 K depend strongly on the solvent density. The characteristic differences in the orientation of water molecules around positive and negative ions in the first solvation shell at 683 K also remain the same as at room temperature, except for the large I^+ and I^-, for which the hydration has a strong hydrophobic component.

We conclude that hydrophilic hydration due to ion−solvent interactions is relatively insensitive to changes in temperature and solvent density, while hydrophobic solvation, associated with cage formation around a solute, is sensitive to both temperature and solvent density. This is particularly so in the supercritical region where high solvent compressibility allows the solvent density to be changed easily with pressure.

The partial molar volume of a solute in solution can be positive or negative. The sign of this property is determined by the magnitude of the integral of the solute−solvent direct correlation function. Uncharged solutes have positive partial molar volumes, while ions tend to have negative values in the supercritical region. We have discussed a simple approximation for the partial molar volumes of uncharged solutes in which the integral of the solute−solvent direct correlation function is replaced by twice the second virial coefficient for the corresponding potential. The approximation is less satisfactory for charged solutes but becomes more accurate when the parameter ($\beta q\mu/\sigma_{io}^2$) is small. If the ion−solvent potential is approximated as a charge dipolar hard-sphere interaction, then the integral which governs the sign of the partial molar volume can be determined analytically in the mean spherical approximation,[28−30] but electrostriction effects would be excluded from such a linear theory. This is not the case with the second virial coefficient, which is nonlinear in the potential. Improved approximations that take into account electrostriction[31,32] can be employed to determine the partial molar volumes and structural details of simple ions and uncharged solutes. We plan to discuss this in a future study.

The thermodynamics of solvation as a continuous function of the charge and size of ions at 298 K has been analyzed by Lynden−Bell and Rasaiah using an extended Lagrangian for the system.[16] Their discussion of the entropy of solvation provides a detailed microscopic picture of cage formation around neutral solutes and large ions and the asymmetry in the hydrophilic solvation of cations and anions in water. It would be desirable to extend the study to solutes at different solvent densities in the supercritical region of water. A comprehensive explanation will also require additional studies of hydrogen-bonding dynamics of the cages and the entropy of solvation. Solvation studies in non-hydrogen-bonded solvents will also be of great interest.

The dynamics of hydration shells is strongly influenced by temperature and solvent density, even when their structures are relatively insensitive to these factors. This aspect of solvation, which influences the transport coefficients of the solutes, is discussed in the following paper.[33]

Acknowledgment. This study was supported by grants from the National Science Foundation, CHE 99610288 and CHE 9961336, to J.C.R. We thank Dr. J. M. H. Levelt Sengers for helpful correspondence and clarification of the thermodynamic properties of solutions near the critical point of the solvent. The hospitality of Drs. J. Hubbard, Anne Plant, R. Mountain, and M. Gilson at the National Institute of Standards and Technology at Gaithersburg, MD, and at the Center for Advanced Research in Biotechnology at Rockville, MD, during the summer of 1999 is most gratefully acknowledged. We thank an anonymous reviewer and Alexander (Sasha) M. Berezhkovski for their incisive comments.

JA001978Z

(28) Wertheim, M. *J. Chem. Phys*. **1971**, *55*, 4291.
(29) Chan, D. Y. C.; Mitchell, D. J.; Ninham, B. W. *J. Chem. Phys*. **1979**, *70*, 2946.
(30) Zhu, J.; Rasaiah, J. C. *J. Chem. Phys*. **1989**, *91*, 505.
(31) Rasaiah, J. C.; Isbister, D.; Stell, G. *J. Chem. Phys*. **1981**, *75*, 4707.
(32) Rasaiah, J. C. *J. Chem. Phys*. **1982**, *77*, 5710.
(33) Noworyta, J. P.; Koneshan, S.; Rasaiah, J. C. *J. Am. Chem. Soc.* **2000**, *122*, 11194−11202.